

Analysis of WorldView-3 Satellite Imagery for the Andrew Lake Area, Northeastern Alberta

AER/AGS Special Report 123

Analysis of WorldView-3 Satellite Imagery for the Andrew Lake Area, Northeastern Alberta

B. Rivard and J. Feng

Department of Earth and Atmospheric Sciences, University of Alberta

February 2025

©His Majesty the King in Right of Alberta, 2025
ISBN 978-1-4601-5724-4

The Alberta Energy Regulator / Alberta Geological Survey (AER/AGS), its employees and contractors make no warranty, guarantee, or representation, express or implied, or assume any legal liability regarding the correctness, accuracy, completeness, or reliability of this publication. Any references to proprietary software and/or any use of proprietary data formats do not constitute endorsement by the AER/AGS of any manufacturer's product.

If you use information from this publication in other publications or presentations, please acknowledge the AER/AGS. We recommend the following reference format:

Rivard, B. and Feng, J. (2025): Analysis of WorldView-3 satellite imagery for the Andrew Lake area, northeastern Alberta; Alberta Energy Regulator / Alberta Geological Survey, AER/AGS Special Report 123, 19 p.

Publications in this series have undergone only limited review and are released essentially as submitted by the author.

Authors address:

B. Rivard and J. Feng
Department of Earth and Atmospheric Sciences
University of Alberta
1-26 Earth Sciences Building
Edmonton, AB T6G 2E3
Canada

Tel: 780.953.7110
Email: bentrivard9@gmail.com

Published February 2025 by:

Alberta Energy Regulator
Alberta Geological Survey
Suite 205
4999 – 98 Avenue NW
Edmonton, AB T6B 2X3
Canada

Tel: 780.638.4491
Email: AGS-Info@aer.ca
Website: ags.aer.ca

Foreword

As part of the Alberta Minerals Strategy and Action Plan, the Alberta Energy Regulator / Alberta Geological Survey acquired Maxar WorldView-3 satellite imagery over the Canadian Shield in northeastern Alberta. This acquisition aimed to support the detection and mapping of metallic mineral occurrences, where documented deposits of gold, base metals, uranium, and rare-earth elements are found in narrow belts associated with major shear zones.

In March 2024, Professor Emeritus Benoit Rivard and Dr. Jilu Feng were contracted to conduct a detailed analysis of WorldView-3 satellite imagery of the Andrew Lake area, building on previous work in the Leland Lakes area. This study sought to identify mineralization potential by detecting exposed rock outcrops, delineating lithological units, and mapping mineral alteration features within the Alberta Shield.

This report presents key findings that expand the understanding of the lithological and mineral alteration patterns within the Andrew Lake region. The analysis identified zones with significant internal variability within primary rock units, particularly in the Taltson basement and Rutledge River complexes. These zones revealed high concentrations of minerals such as white mica, biotite, and chlorite. Through the use of a ‘White mica index’ and a ‘White mica / Chlorite-biotite index,’ previously unidentified areas rich in hydroxyl-bearing minerals were detected. These minerals are present in biotite schists, amphibolite, and garnetiferous layers. This highlights mineralogical diversity that points to potential subunits within the primary mapped units.

Preprocessing involved masking non-rock features such as vegetation, water, burns, and shadows to refine the detection of rock outcrops. Key spectral indices were applied to analyze iron- and hydroxyl-bearing minerals, facilitating the distinction between mafic and felsic lithologies. Spectral angle mapping (SAM) was used with both image-derived and field-collected endmembers, yielding detailed spectral maps that highlighted zones of potential mineralization and specific lithological contrasts.

This report’s findings underscore the potential of WorldView-3 imagery for accurately mapping complex lithological features and identifying zones of mineralization, particularly in areas with extensive vegetation cover. Field validation is recommended to confirm remote sensing interpretations and to refine exploration strategies in northeastern Alberta.

Aside from the cover, copyright information, and this page, the report is published as received from the vendor (with minor editing).

This work was completed under the Mineral Grant provided by the Government of Alberta dated June 22, 2021.

AER Service Agreement 23SA-SR007

Analysis of WorldView-3 satellite imagery for the Andrew Lake area, Alberta

By

Professor Emeritus Benoit Rivard and Dr. Jilu Feng

benoitrivard9@gmail.com, 780-953-7110

Jfeng@ualberta.ca

March 25, 2024

Contents

Foreword.....	iv
1 Introduction.....	1
2 Satellite data.....	1
3 Methods.....	3
3.1 Masking.....	4
3.2 Generation of an outcrop map.....	4
3.3 Extraction of lithological information.....	4
4 Results.....	7
4.1 Outcrop map.....	7
4.2 Geologic background and index images.....	7
4.3 Possible links between map units and index image domains.....	10
4.4 Possible links between map units and image endmember maps.....	13
4.5 Possible links between map units and Halo (field spectra) endmember maps.....	16
5 Discussion and conclusion.....	17
5.1 Image acquisition.....	17
5.2 Lithological inferences.....	17
6 References.....	18
7 Appendix 1: List of digital deliverables.....	19

Figures

Figure 1. Google map view with red polygon located in the northwest corner of the province of Alberta and defining the area of interest encompassed by the WorldView-3 satellite data.....	1
Figure 2. “True color” mosaic of the two WorldView-3 lines encompassing the area of interest. Disparities in the state of the vegetation are apparent between the June 2022 scene on the left and the October 2021 scene on the right where senescence is occurring.....	2
Figure 3. Example misalignment of VNIR and SWIR data seen along the left and right side of the June 2022 scene shown on the left and on the left side of the October 2021 scene shown on the right.....	3
Figure 4. Example WorldView-3 spectra showcasing a strong iron (Fe) absorption near 900 nm (red spectrum) and a strong hydroxyl (OH ⁻) absorption near 2200 nm (white spectrum).....	5
Figure 5. Outcrop map for field planning and used for lithological analysis.....	7
Figure 6. Geologic map (centre) along with legend (right) taken from Panã and Prior (2010) and the WM/Chl-Bio index image (left). Note that the map does not cover the southern portion of the imaged area. Three areas highlighted by a red polygon are enlarged in subsequent figures. Three lakes (numbers 1, 2, 3) are highlighted on the map (in black) and image (in white) to provide the reader with common reference features.....	9
Figure 7. Key index images with white text labels in lower right corner. Refer to equations 5, 6, and 8 for computation of indices. Red boxes A, B, C, and D mark the location of enlargements shown in Figures 8, 9, 10 and 11 respectively.....	10
Figure 8. Enlargement A on Figure 7. The area present distinctly low (blue) and high (red and yellow) WM/Chl-Bio and White Mica index values respectively that may represent the greater extent of localized hornblende granodiorite (purple map unit) and Rutledge River Complex schists (brown unit) seen on the map.....	11
Figure 9. Enlargement B on Figure 7. The map shows more extensive hornblende granodiorite (purple unit) in the north and small but quite abundant strips of amphibolite (green unit). Red arrows point to two distinct zones of low WM/Chl-Bio (e.g. blue) and high White Mica (e.g. red) index values that clearly track the amphibolite. Yellow arrows point to a large area of similar	

values on both images that cannot be related to a map pattern though there are small lenses of amphibolite shown. 11

Figure 10. Enlargement C on Figure 7 containing a series of outcrops visible in the true color image and uniquely high values in the WM/Chl-Bio index. To the west, a series of outcrops follow a near north south trend (white arrows) that tracks map occurrences of the Rutledge River Complex (brown map unit). The occurrence of a few outcrops in the east (yellow arrows) follows the trace of a fault. 12

Figure 11. Enlargement D on Figure 7. Yellow arrows point to outcrops with elevated white mica index values (pale red areas) likely part of the Ney Lake leucogranite described as containing minor muscovite and biotite..... 13

Figure 12. Thirteen geologically relevant image endmembers. The y-axis reflectance is reflectance DN/100 (e.g. 1000=10%)..... 13

Figure 13. Comparison of spectral angle maps (SAM) derived from image endmembers and different spectral ranges, with the geological map approximately co-registered. White and black letters A and B act as reference point marking the location of Pans Lake and Spider Lake. The SAM map on the left was generated using the full spectral range (427-2329nm, all 16 bands) and a subset of the thirteen endmembers (EM 3,7,11 removed) to focus the analysis on differences in broad spectral shape amongst endmembers including the influence in the strength of iron features. The SAM map on the right was generated using the last four bands in the shortwave infrared and the 13 endmembers to focus the analysis on variations in the strength of hydroxyl features amongst endmembers. Image elements highlighted by yellow and white arrows are discussed in the text..... 14

Figure 14. Enlargement from the SAM map (SWIR range) shown on Figure 13 along with partial coverage of the geological map and a plot of a subset of the thirteen image endmembers used to discuss outcrops seen in areas 1, 2, and 3 encompassing red, magenta, and orange pixels respectively. A and B mark the location of Pans Lake and Spider Lake..... 15

Figure 15. Eight Halo reflectance spectra (left) selected to capture a range of spectral characteristics and reflectance amplitude and equivalent spectra after resampling to WorldView-3 bandpasses (right). Note several hydroxyl features in the shortwave infrared attributable in part white mica, biotite, and chlorite whose presence and absorption strength influence the shape of the resampled spectra in the last four bands. 16

Figure 16. Comparison of spectral angle maps (SAM) derived from the eight Halo spectra (see Figure 15) and different spectral ranges, with the geological map approximately co-registered. The SAM map on the left (427-2329nm, all 16 bands) and on the right (2160-2329nm, 4 bands) made use of all eight spectra shown on Figure 15..... 17

1. INTRODUCTION

This report summarizes the analysis of WorldView-3 imagery over the Andrew Lake area of interest in Alberta (Figure 1) as part of AER Service Agreement 23SA-SR007. The area encompasses extensive vegetation cover and the analysis aimed to isolate exposed outcrop, delineate lithologic units and detect and map potential mineral alteration. The limited spectral dimensionality of WorldView-3 data implied a focus on the detection of iron oxides and OH- bearing minerals (e.g. white mica and biotite, chlorite, amphibole as a group). This work is conducted as part of an initiative to detect potential metallic mineral occurrences in the Alberta shield where known occurrences of gold, base metals, uranium, and rare-earth elements have been documented (Godfrey 1958, 1961, 1963, Langenberg and Eccles 1996, Panā and Prior 2010). These mineral occurrences are associated with alteration mineral exposures on the surface such as weathered sulphide horizons, schists, and pegmatites. The satellite data analysis follows the process established for the analysis of WorldView-3 imagery for the Leland Lakes area in 2022-2023 as part of the AER/AGS Special Report 116.

2. SATELLITE DATA

Two lines of WorldView-3 satellite data acquired in October 16, 2021 and June 8, 2022, encompass the area of interest in northern Alberta (Figure 1). Each line was delivered as two datasets. The visible near infrared data (VNIR) has 8 spectral bands centered nominally at 427, 482, 547, 604, 660, 723, 824, and 914 nm with a spatial resolution of 1.24 m. The shortwave infrared data (SWIR) has 8 spectral bands centered nominally at 1209, 1572, 1661, 1730, 2164, 2202, 2259, and 2329 nm with a spatial resolution of approximately 4 m. Preprocessing of the data conducted by the data provider included an atmospheric correction (ACOMP) with SCA correction applied to both datasets to minimize stripping, a standard orthorectification with nearest neighbour resampling, and an alignment correction (i.e. a boresight correction) for both dataset to enable their joint analysis. The data delivered is thus orthorectified imagery at surface reflectance and the SWIR data is resampled to 1.24 m to provide a 16-band spectrum per 1.24 m pixel. Figure 2 is a “true color” mosaic (995 km²) of the two lines encompassing the area of interest.

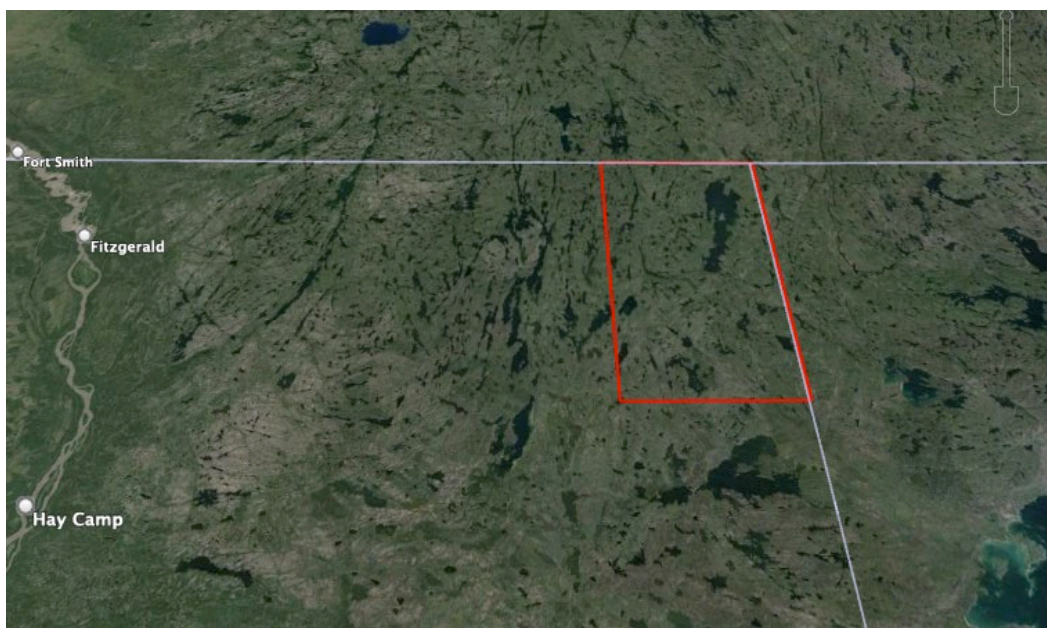


Figure 1. Google map view with red polygon located in the northwest corner of the province of Alberta and defining the area of interest encompassed by the WorldView-3 satellite data.

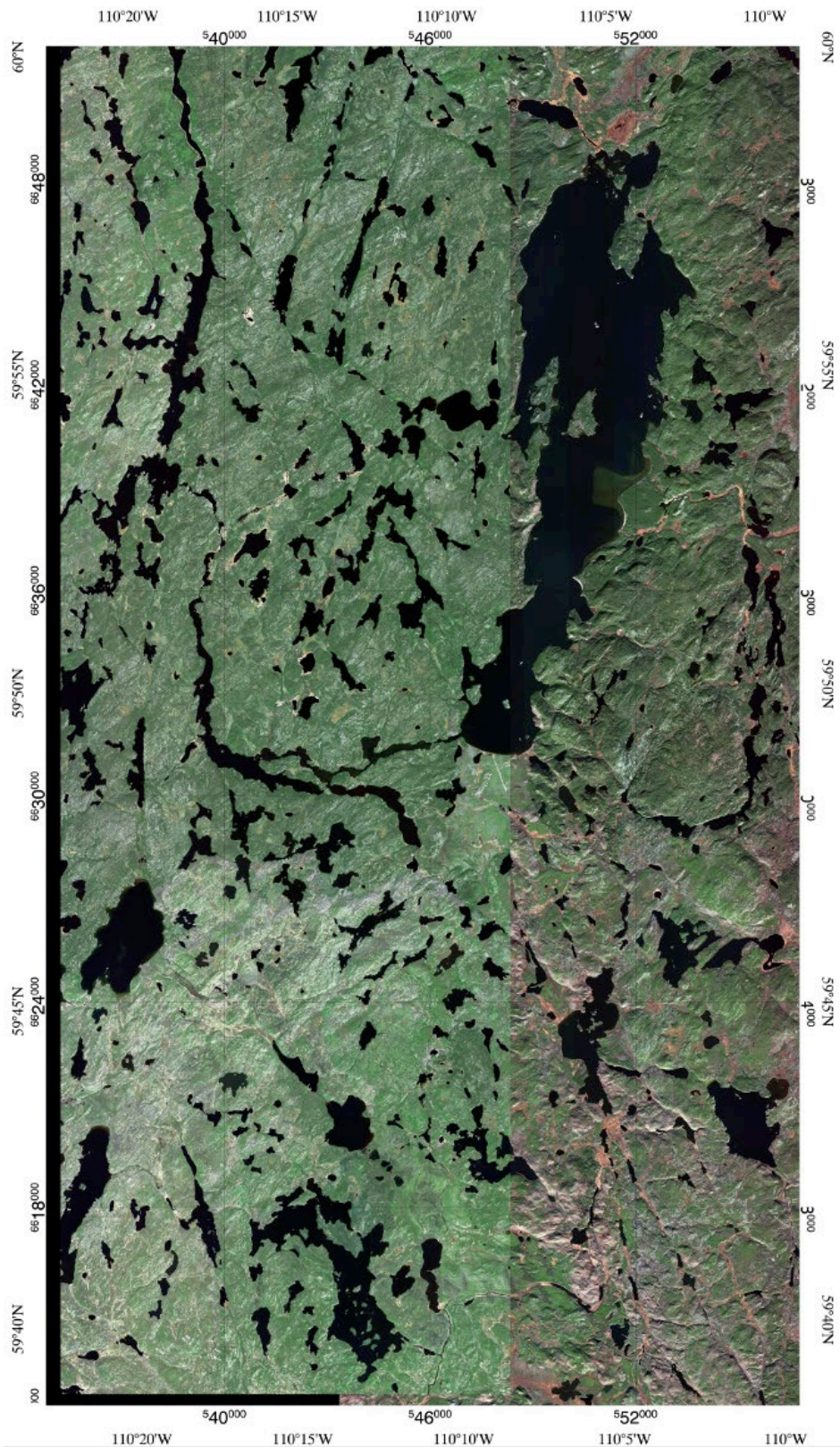


Figure 2. “True color” mosaic of the two WorldView-3 lines encompassing the area of interest. Disparities in the state of the vegetation are apparent between the June 2022 scene on the left and the October 2021 scene on the right where senescence is occurring.

Despite the corrections listed above there remained a misalignment of VNIR and SWIR data noted on the borders of each line, as seen in Figure 3. Consequently, when the mosaic of the two lines was assembled for varying products, portions of each line encompassing misalignment were removed and use of the June 2022 scene was maximized as it revealed more outcrop. This ensured removal of alignment errors in the mosaic and derived products.

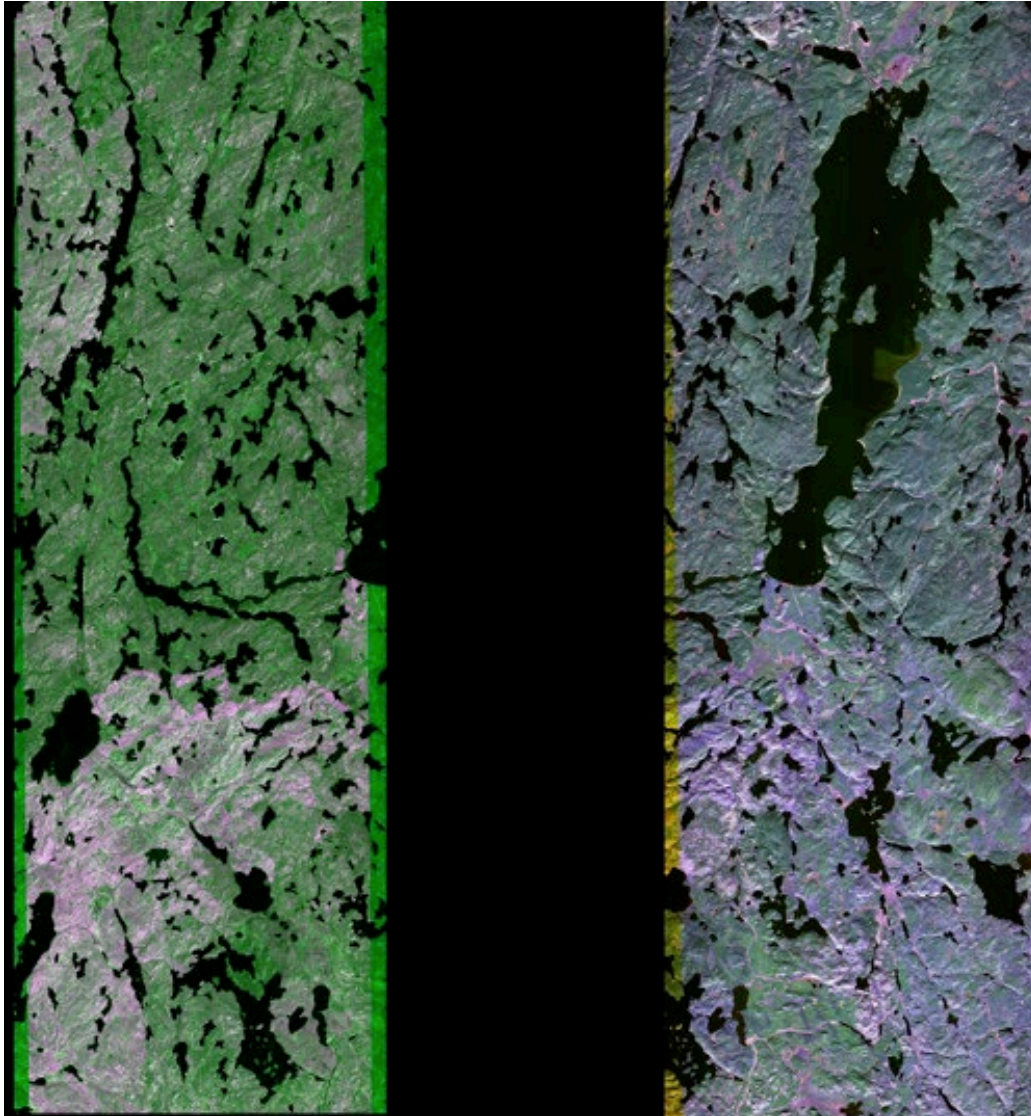


Figure 3. Example misalignment of VNIR and SWIR data seen along the left and right side of the June 2022 scene shown on the left and on the left side of the October 2021 scene shown on the right.

3. METHODS

Several image processing methods were used, first to isolate pixels occupied by outcrop and generate an outcrop distribution map, and then to extract lithological information. The first set of methods relate to the generation of an outcrop map and involve masking all pixels not occupied by outcrop and those include

pixels affected by clouds, water, vegetation, burns, and in shadow. The second category of methods includes the computation of spectral indices, the extraction and analysis of image spectral endmembers, and the analysis of reflectance spectra collected in the field all aiming to highlight lithological/alteration information.

3.1 Masking

Four masks (Equations 1-4) were designed for masking of vegetation, clouds, water, burns and shadows. A normalized vegetation index (Equation 1) was calculated for every pixel in the VNIR data to mask standing water (e.g., lakes, rivers), vegetation, and clouds. The Shadow index (Equation 2) (Shedlovska and Hnatushenko 2019) and Burn index (Equation 3) minimize the impact of shadows (including cloud shadows) and recent fire scars. The albedo (Equation 4) mask was also found to help delineate outcrops when dealing with two scenes with different solar illumination angles impacting shadows. For this index focus is given to bands in the shortwave infrared where outcrops have highest reflectance, specifically from band 7 (830 nm) to band 17 (2330 nm). The value of 5000 is used to scale the results to 0-1.

$$\text{Equation (1) NDVI index} = (\text{VNIR 7} - \text{VNIR 5}) / (\text{VNIR 7} + \text{VNIR 5})$$

$$\text{Equation (2) Shadow index} = (\text{VNIR 8} - \text{VNIR 2}) / (\text{VNIR 8} - \text{VNIR 2}) - \text{VNIR 7}$$

$$\text{Equation (3) Burn index} = (\text{VNIR 1} + \text{VNIR 2} + \text{VNIR 3}) / 3$$

Equation (4) for Albedo

$$\text{Albedo} = \frac{1}{10.0} * \sum_{\text{band}=7}^{16} \frac{DN^{\text{band}}}{5000.0}$$

3.2 Generation of an outcrop map

To derive an outcrop distribution map from which the lithological/alteration analysis could be conducted, the following thresholds were used: pixels were retained if the NDVI was greater than 0.01 (water mask), the Burn index > 0.06, and the Shadow index < 0.5. In addition, pixels were retained if NDVI > 0.3 for the June scene and > 0.35 for the October scene. Lastly pixels were retained if the Albedo > 0.34 for the June scene and > 0.46 for the October scene.

3.3 Extraction of lithological information

3.3.1 Indices

As described in the AER/AGS Special Report 116 for the Leland Lakes area, three indices were devised to capture mineralogical and thus lithological information related to the presence of hydroxyl (OH⁻) and iron (Fe³⁺) bearing minerals (e.g., white mica and iron oxides, Mars (2018)) seen in WorldView-3 image spectra (Figure 4).

The “White Mica index” is listed in Equation 5 and consists of a normalized ratio of two bands (SWIR5, SWIR6) at 2164 and 2202 nm respectively and thus capitalises on the white mica absorption feature located nominally at 2200 nm. Its intent is to inform on the relative abundance of white mica. The “Rock MF (Mafic Felsic)” index and the “Rock Fe (iron)” index are listed in Equation 6 and 7 respectively. The Rock Fe is designed specifically to measure the strength of the iron absorption nominally centered on band VNIR 7 located near 900 nm. Specific to this study we include a fourth index (named WM/Chl-Bio

in Equation 8) that consists of a normalized ratio of the SWIR bands 5 (2164 nm) and 8 (2329 nm) and thus contrasts the strength of the white mica absorption to that of chlorite and biotite as a group (Mg-OH feature).

$$\text{Equation (5) White Mica} = (\text{SWIR 5} - \text{SWIR 6}) / (\text{SWIR 5} + \text{SWIR 6})$$

$$\text{Equation (6) Rock MF} = (\text{VNIR 3} + \text{SWIR 3}) / (\text{VNIR 5} + \text{VNIR 7})$$

$$\text{Equation (7) Rock Fe} = ((\text{VNIR 6} - \text{VNIR 7}) / (\text{VNIR 6} + \text{VNIR 7})) + ((\text{VNIR 8} - \text{VNIR 7}) / (\text{VNIR 8} + \text{VNIR 7}))$$

$$\text{Equation (8) WM/Chl-Bio} = (\text{SWIR 5} - \text{SWIR 8}) / (\text{SWIR 5} + \text{SWIR 8})$$

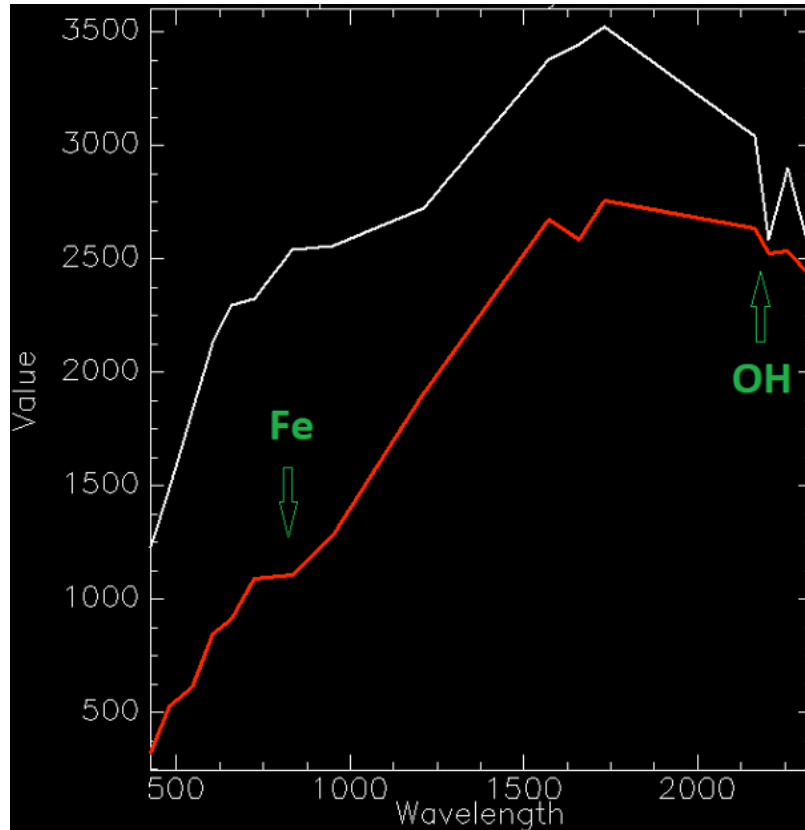


Figure 4. Example WorldView-3 spectra showcasing a strong iron (Fe) absorption near 900 nm (red spectrum) and a strong hydroxyl (OH⁻) absorption near 2200 nm (white spectrum).

3.3.2 Use of image endmembers

The use of spectral endmembers is one approach to explore the data for lithologic information. Endmembers represent “purest” spectra of representative materials in the scene. Endmembers can be collected in the field or laboratory from known surfaces (outcrop or samples respectively) or extracted from imagery. The latter is commonly preferred for two reasons: 1) laboratory and field spectra may not capture all relevant surface components or may be inadequate representations (e.g., fresh rather than exposed weathered surfaces); and 2) image endmembers sample surfaces directly from the scene and are collected under the same viewing and illumination conditions as all spectra in the scene. Image endmembers are assumed to be relatively pure spectra, meaning that minimal mixing with other endmembers has occurred within the pixel.

To derive an image endmember set from the satellite data, we made use of the spatial-spectral endmember extraction (SSEE) method described in Rogge et al. (2007, 2012). The number of endmembers extracted by SSEE is defined by the data. SSEE comprises three steps. The image is first divided into equal sized non-overlapping subset regions and a set of eigenvectors that explain the majority of spectral variance is calculated for each subset via singular value decomposition. In the second step the image data are projected onto the local eigenvectors compiled from all subset regions and those pixels that lie at extremes of the vectors are retained as candidate endmembers. The third step averages the candidate pixels with all other pixels within a given spatial window that are also spectrally similar based on a similarity metric, such as spectral angle (Price, 1994). SSEE generally finds several endmembers and many that are similar but spatially independent. Geologically relevant endmembers were obtained and as discussed in the results, these were used as input to the Spectral Angle Mapper (SAM) tool to capture what appeared to be spatially continuous and significant areas (e.g., lithologic units). Different combinations of endmembers and different spectral ranges were explored, the latter to examine the contrast in the overall spectral shape of endmembers (e.g., examining full spectral range) and to enhance subtle differences amongst spectra in the region where hydroxyl features are observed (e.g., examining the SWIR region).

3.3.3. Use of reflectance spectra collected in the field

During fieldwork conducted in the summer of 2023, AER personnel collected reflectance spectra from weathered outcrop surfaces in the Andrew Lake area using a Terraspec Halo portable spectrometer equipped with a contact probe. As part of this study, some of these spectra were provided for the image analysis and were resampled to the WorldView-3 16 bandpasses prior to their use with the Spectral Angle Mapper (SAM).

4. RESULTS

4.1 Outcrop map

The outcrop map generated from the WorldView-3 data is shown in Figure 5 and reveals the presence of considerable outcrop in the area. There is an apparent east-west bias in the extent of outcrop revealed by the analysis of the WorldView-3 data which is introduced by the disparity in illumination (extent of shadowing) and vegetation phenology (senescence in the fall scene) between the two available scenes. The scene captured in June, which occupies the left half of the map, revealed more outcrop. The region with anomalously high outcrop exposure in the southwest and northwest corners of the map area may relate to past forest fires enhancing outcrop detection from satellite imagery.

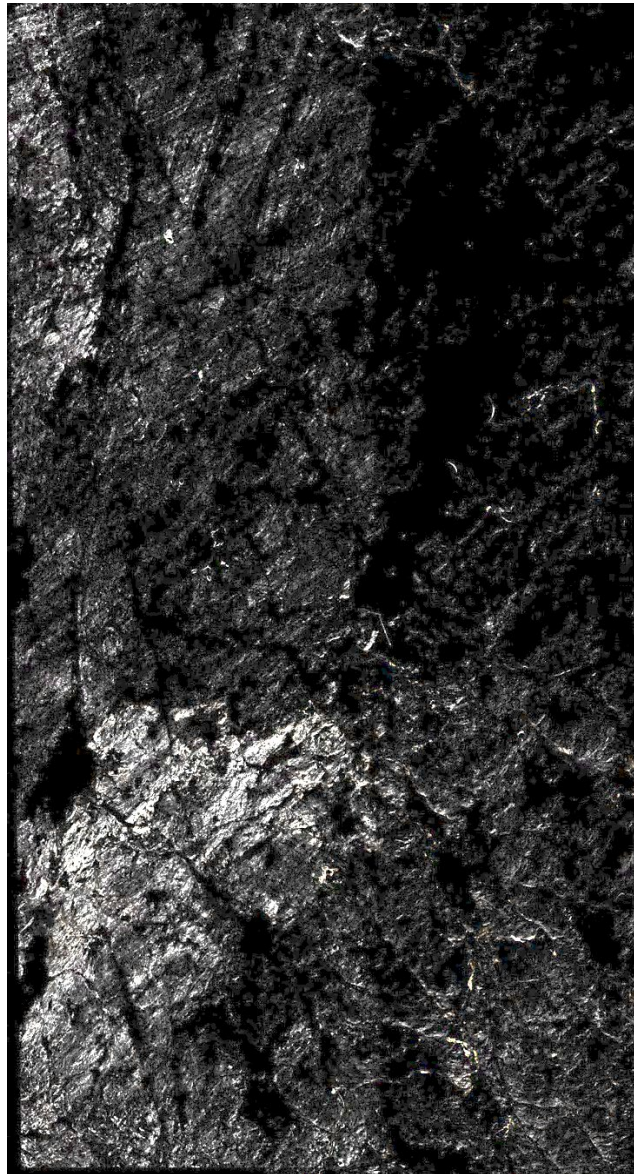


Figure 5. Outcrop map for field planning and used for lithological analysis.

4.2 Geologic background and index images

The Andrew Lake area occupies the northeastern corner of the Alberta Shield and has been identified since the 1950's for its mineral potential particularly for uranium. The general geology of the area has been

described in several reports most significantly starting from those of Godfrey (1958, 1961, 1963) and more recently by Langenberg and Eccles (1996) and Panã and Prior (2010). Here we refer extensively to the latter publication and associated most detailed compilation geological map that summarizes the geological context and main map units in the Andrew Lake area as we explored potential links between map units and observations from WorldView-3 image products.

As part of the results, we present a suite of image products described in the methods, first for the total area covered by imagery and then for specific subsets of interest. We also make observations from these products in support of lithological inferences. An inherent challenge in the interpretation of such products is the environment that was imaged, which is partially forested and can lead to false image interpretations despite best efforts to remove the influence of vegetation in imagery. In addition, as indicated in section 4.1, imagery obtained at different times of the year offer different potential for capturing outcrops. In this case there are clearly poorer results in terms of outcrop recovery in the October scene covering the eastern parts of the map area which impacts lithological inferences.

Another inherent challenge is the nature of the geology of the area that has a predominance of felsic rocks that may display limited spectral diversity (e.g., similar mineralogy). Also, varying schists and amphibolites that can harbor hydroxyl-bearing minerals (e.g. white mica, biotite, chlorite, amphiboles), of known remote sensing detection potential, are challenging to convey on maps as they occur at a variety of scales and are of varying continuity. This can limit inferences between image domains and a map that may not always convey their occurrence. In a prior study of WorldView-3 imagery for the Leland Lakes area in 2022-2023, as part of the AER/AGS Special Report 116, we benefited from a detailed map at a scale of 1:31680 (Tulip Lake district) to focus the links between image interpretation and documented maps units. The current study does not benefit from such geological detail putting further importance in the field validation of inferences offered here. Our approach for this report is to establish potential correlations between map units and image domains, assign potential lithologic labels to image observations with the recognition that such observations will need field validation.

As stated in Panã and Prior (2010), and in reference to the map and legend shown in Figure 6 taken from this report, the four principal rock groups occurring in the Andrew Lake area are, in chronological order: 1) the Taltson basement complex, 2) the Rutledge River Complex, 3) the Waugh Lake Complex, and 4) the Taltson plutonic complex. Granitoid gneiss of the Taltson basement complex occupy more than the western half of the study area and encompass leucocratic granite, mylonites, hornblende granodiorite and biotite granite gneiss. Of potential significance to image interpretation, they also include biotite schists, amphibolite, hornblendite and garnetiferous layers (see purple and green map units). The Rutledge River Complex (pale brown map unit) is a migmatitic complex encompassing biotite+garnet+aluminosilicate gneiss and schists interlayered with granite and pegmatite and small amphibolite and mafic lenses. Results of retrogression include chlorite-sericite schists and phyllonite. The mineralogy of the schists and mafic rocks also offer a potential remote detection of this map unit. Panã and Prior (2010) refer to the Waugh Lake Complex as an extensive belt of low grade metamorphic tectonite encompassing a suite of mafic rocks, schists, and phyllonites of potential for remote detection but entirely exposed in the October WorldView scene with poorer detection potential. The Taltson plutons also primarily occupy the map portion covered by the October scene and encompass two plutonic suites of biotite granites (Andrew Lake and Colin Lake). The geologic summary above puts an emphasis on rock types and related map units that offer the best potential of detection from WorldView-3 imagery and the reader is encouraged to refer to Panã and Prior (2010) for a more complete description of the map units including metamorphic history and geochronology. The portion of the geologic map shown in Figure 6 also includes several mineral occurrences with high radioactivity (locations 1,2,3a-d, 6, and 8 shown in red) described in Panã and Prior (2010). Note that the map does not cover the southern portion of the imaged area. Shown in Figure 6 is the WM/Chl-Bio index because it highlights several regions (red polygons) with variability in index values. Three lakes (numbers 1,2,3) are highlighted on the map (in black) and image (in white) to provide the reader with common reference features.

The WM/Chl-Bio index image is repeated in Figure 7 and juxtaposed to the White Mica and Rock MF images. In all instances the index values are displayed using a rainbow color table shown in Figure 8 with red allocated to highest values. The purpose of Figure 7 is to showcase four areas where variability in index values is observed and of potential interest. Areas A and B are highlighted on all three index images, likely attributable to the greater extent of outcrop captured in imagery (see Figure 5). Area C and D are uniquely highlighted in the WM/Chl-Bio and White Mica image respectively. Subsequent figures (Figures 8-10) provide image enlargements of these areas and related portions of the geologic map.

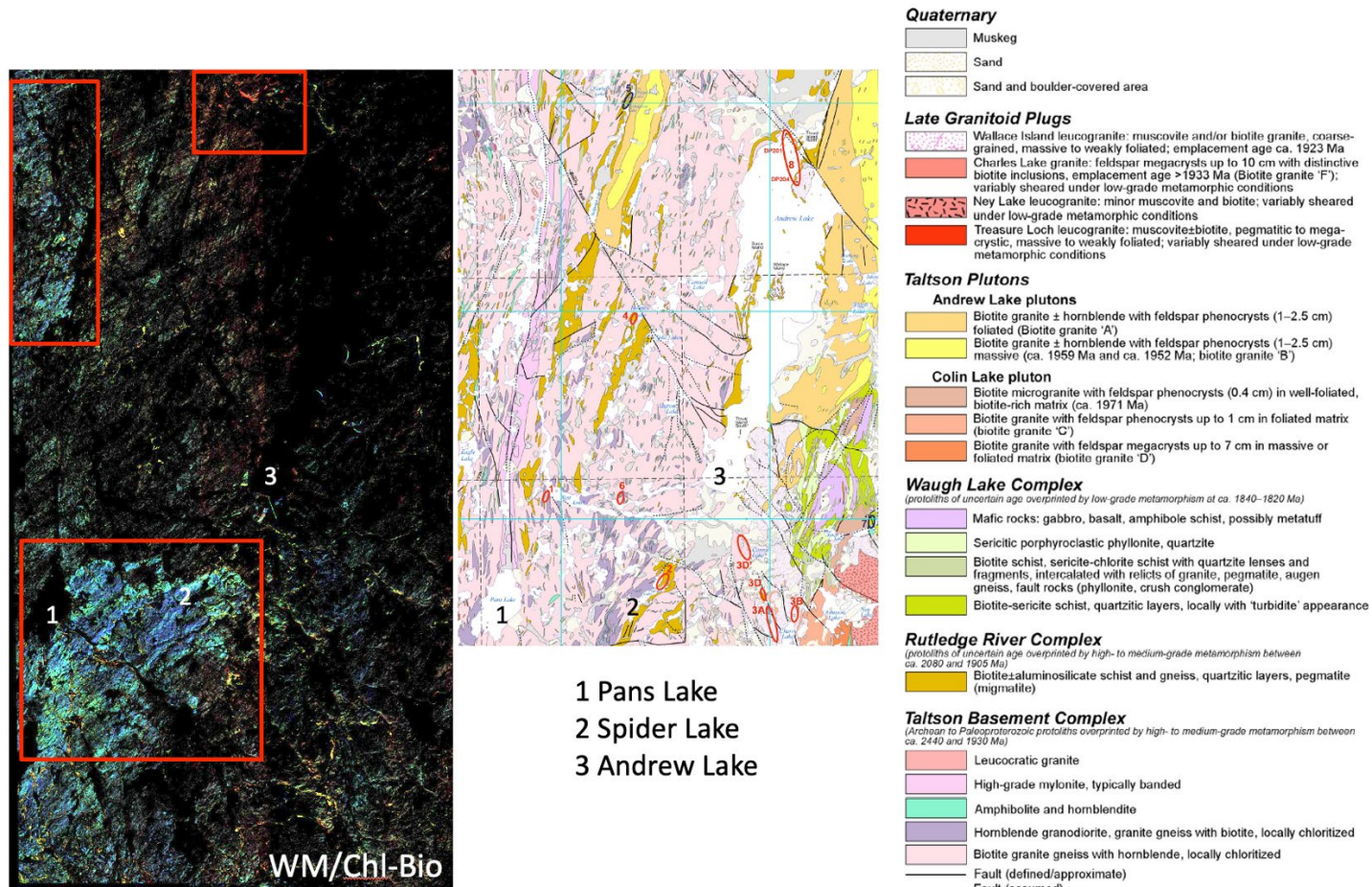


Figure 6. Geologic map (centre) along with legend (right) taken from Panā and Prior (2010) and the WM/Chl-Bio index image (left). Note that the map does not cover the southern portion of the imaged area. Three areas highlighted by a red polygon are enlarged in subsequent figures. Three lakes (numbers 1, 2, 3) are highlighted on the map (in black) and image (in white) to provide the reader with common reference features.

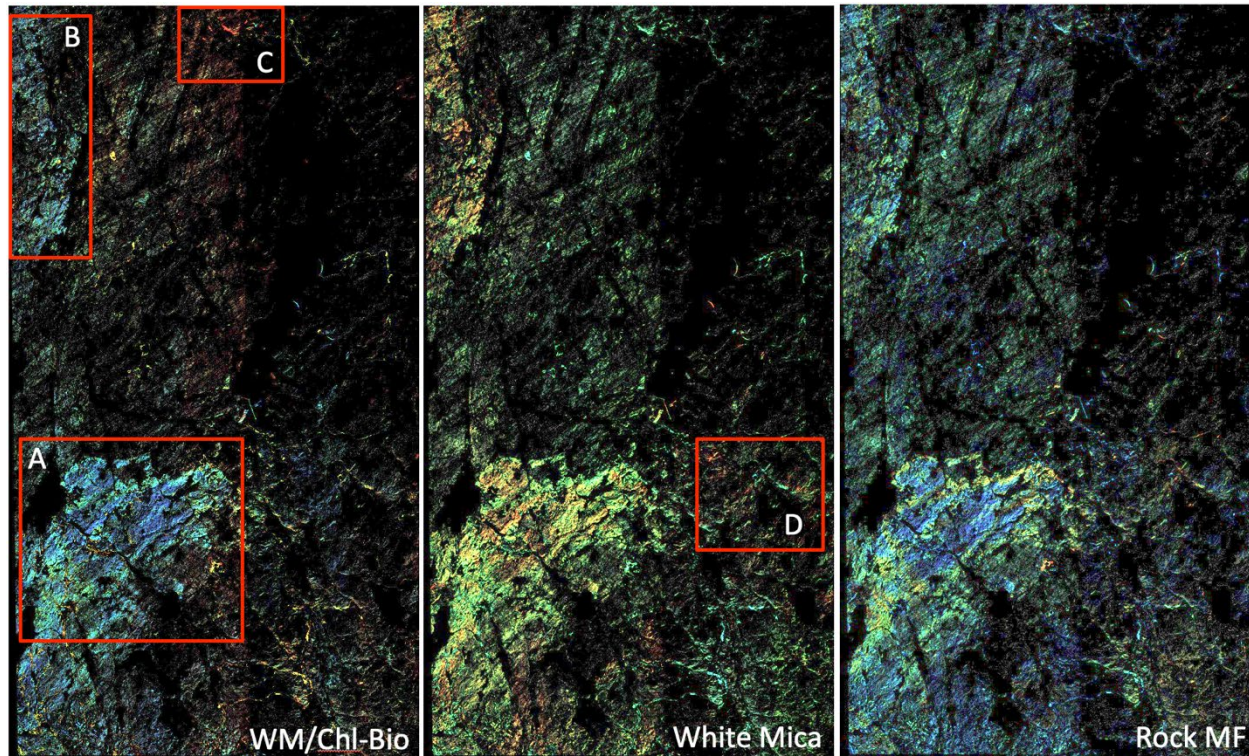


Figure 7. Key index images with white text labels in lower right corner. Refer to equations 5, 6, and 8 for computation of indices. Red boxes A, B, C, and D mark the location of enlargements shown in Figures 8, 9, 10 and 11 respectively.

4.3 Possible links between map units and index image domains

4.3.1 Observations for the western half of the imaged area

Areas A and B of Figure 7 are shown on Figures 8 and 9 respectively and share common characteristics encompassing outcrop regions of elevated (e.g. orange) yet variable (e.g. yellow) white mica index corresponding to low (e.g. blue) yet variable (e.g. green) WM/Chl-Bio index. For area A (Figure 8) the map shows more extensive hornblende granodiorite (purple unit) and extensive stretch of the Rutledge River Complex (brown unit) particularly around Spider Lake. These map units are all described as favoring the presence of biotite which is somewhat inconsistent with the observed index value variability, but the differing scale of representation of imagery and geologic map can make detailed correlations challenging. For area B (Figure 9) the map also shows more extensive hornblende granodiorite (purple unit) and small but quite abundant strips of amphibolite (green unit). Here red arrows point to two distinct zones of low WM/Chl-Bio (e.g. blue) and high White Mica (e.g. red) index values that clearly track the mapped amphibolite. Again, this should point to relatively higher white mica to biotite+chlorite compared to background and is difficult to align with the expected mineralogy of amphibolites but the spatial correlation here appears clear. Yellow arrows point to a large area of similar values on both images that cannot be related to a map pattern though there are small lenses of amphibolite shown. Here perhaps the map does not convey the level of detail necessary for a correlation.

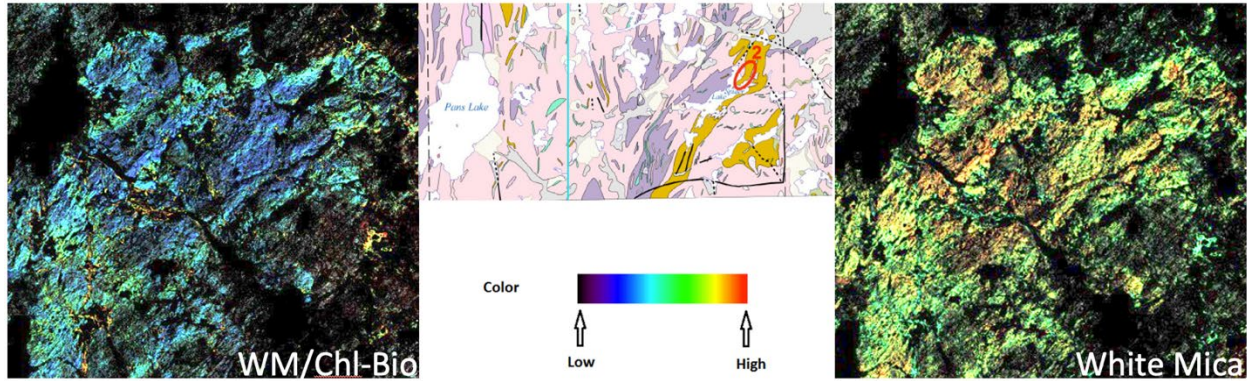


Figure 8. Enlargement A on Figure 7. The area present distinctly low (blue) and high (red and yellow) WM/Chl-Bio and White Mica index values respectively that may represent the greater extent of localized hornblende granodiorite (purple map unit) and Rutledge River Complex schists (brown unit) seen on the map.

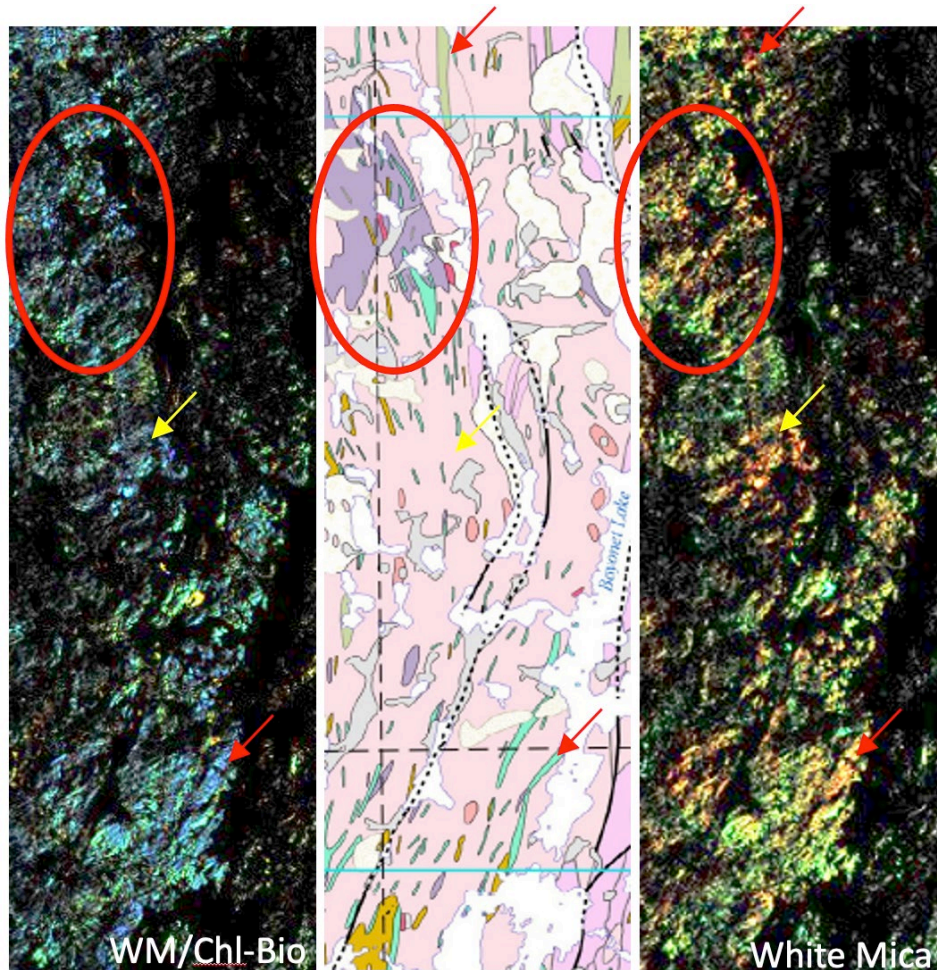


Figure 9. Enlargement B on Figure 7. The map shows more extensive hornblende granodiorite (purple unit) in the north and small but quite abundant strips of amphibolite (green unit). Red arrows point to two distinct zones of low WM/Chl-Bio (e.g. blue) and high White Mica (e.g. red) index values that clearly track the amphibolite. Yellow arrows point to a large area of similar values on both images that cannot be related to a map pattern though there are small lenses of amphibolite shown.

4.3.2 Observations for the north central part of the imaged area

Areas C on Figure 7 is shown in enlargement on Figure 10. It contains a series of outcrops visible in the true color image that present uniquely high values in the WM/Chl-Bio index, therefore unusual high white mica abundance compared to chlorite+biotite. These areas are also highlighted in the White Mica and Rock MF images (Figure 7) along with several other areas, but they are unique in the WM/Chl-Bio image. To the west, a series of outcrops follow a near north south trend (white arrows) that track map occurrences of the Rutledge River Complex (brown map unit) but outcrops further north and east cannot readily be tied to map units though several lenses of amphibolite (green unit) and hornblende granodiorite (purple unit) can be seen nearby. The unique character of these outcrops on the WM/Chl-Bio image and the occurrence of a few outcrops in the east (yellow arrows) that follow the trace of a fault may require a different explanation, possibly the occurrence of pegmatites rich in white mica.

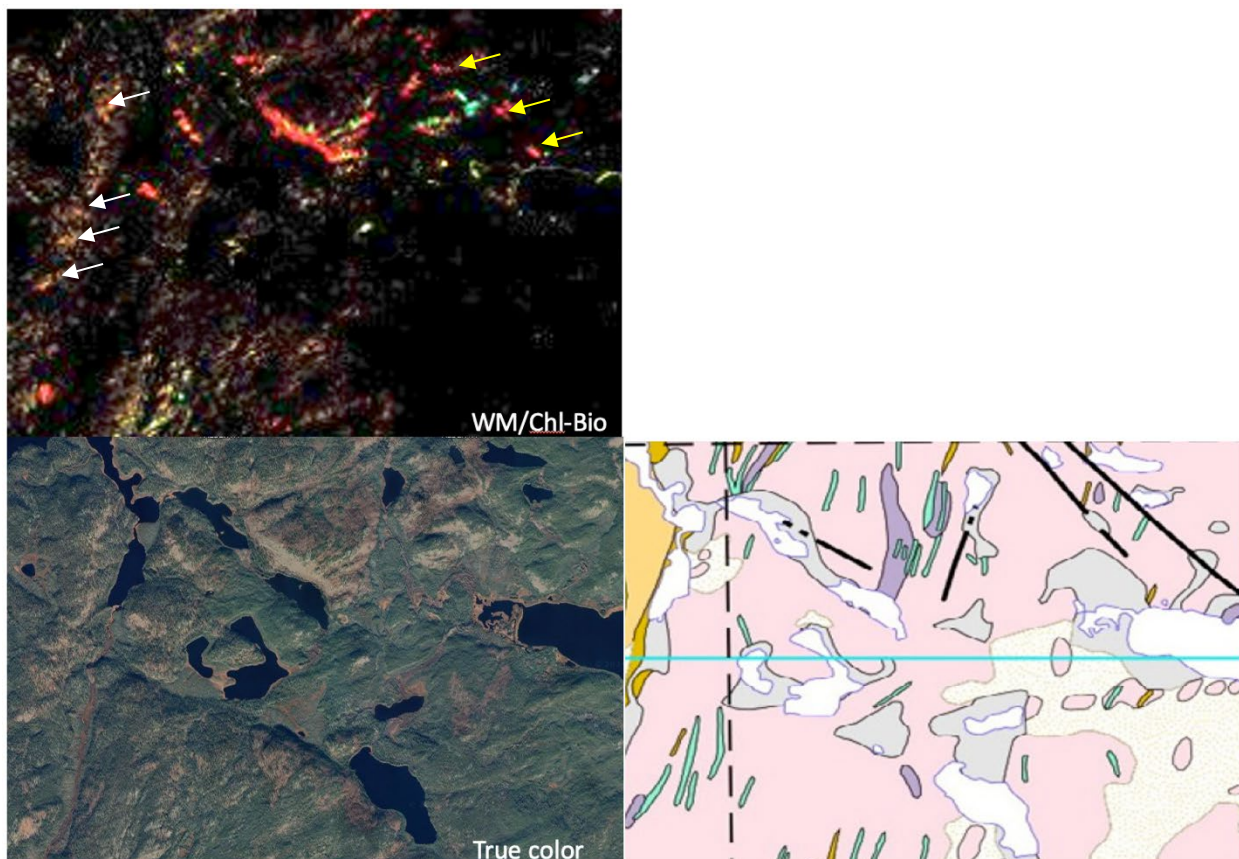


Figure 10. Enlargement C on Figure 7 containing a series of outcrops visible in the true color image and uniquely high values in the WM/Chl-Bio index. To the west, a series of outcrops follow a near north south trend (white arrows) that tracks map occurrences of the Rutledge River Complex (brown map unit). The occurrence of a few outcrops in the east (yellow arrows) follows the trace of a fault.

4.3.3 Observations for the eastern part of the imaged area

Little geological inferences could be obtained from the October scene and thus from the eastern parts of the area. However, areas D on Figure 7, shown in enlargement in Figure 11, displays several outcrops with elevated White Mica index values (pale red areas, yellow arrows) likely part of the Ney Lake leucogranite described as containing minor muscovite and biotite.

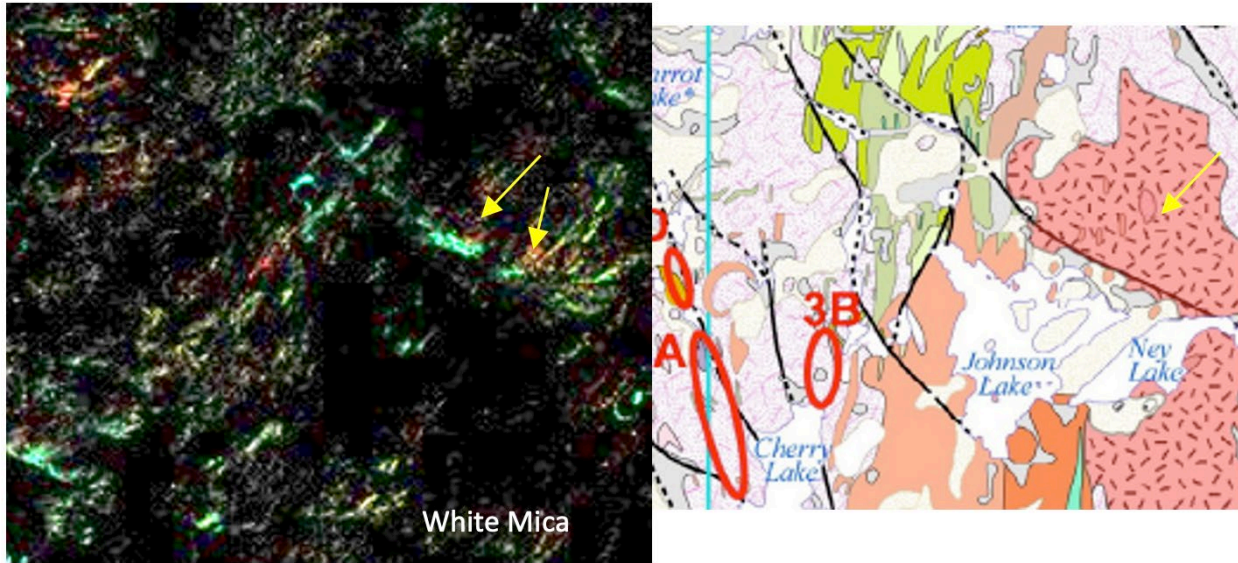


Figure 11. Enlargement D on Figure 7. Yellow arrows point to outcrops with elevated white mica index values (pale red areas) likely part of the Ney Lake leucogranite described as containing minor muscovite and biotite.

4.4 Possible links between map units and image endmember maps

Thirteen geologically relevant image endmembers, shown in Figure 12, were obtained from the endmember extraction process described in section 3.3.2. These were then used to generate spectral angle maps (one for each endmember) that were combined as a color product where each pixel is assigned to the endmember (one color per endmember) with the smallest spectral angle to the pixel spectrum.

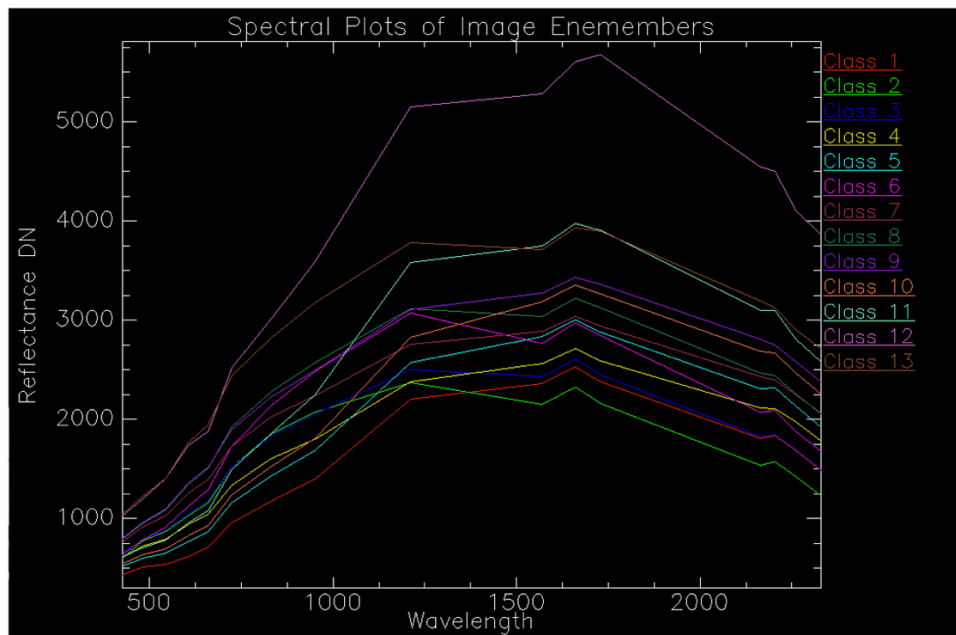


Figure 12. Thirteen geologically relevant image endmembers. The y-axis reflectance is reflectance DN/100 (e.g. 1000=10%).

Two SAM color maps derived from different spectral ranges are shown on Figure 13 with the geological map approximately co-registered. The SAM map on the left (427-2329 nm, all 16 bands) includes ten endmembers (EM 3,7,11 removed) to focus the analysis on differences in broad spectral shape differences amongst endmembers including the influence in the strength of iron features. The SAM map on the right was generated using the last four bands in the shortwave infrared and the thirteen endmembers to focus the analysis on variations in the strength of hydroxyl features amongst endmembers. These SAM maps provide further insights into the area shown in Figure 8 using index imagery. White arrows in the left SAM image highlight detailed lenses, all in magenta, but these breakdown into two groups (magenta and orange) in the image to the right. Yellow arrows highlight red pixels defining different areas in the left and right SAM images which may represent variations of a same unit. In the absence of geologic map information, a lithological interpretation cannot be provided. Note that the suite of outcrops uniquely captured in the northern portion of the WM/Chl-Bio index image, as shown in Figure 10 (section 4.3.2), are also visible for the most part in the right image on Figure 13.

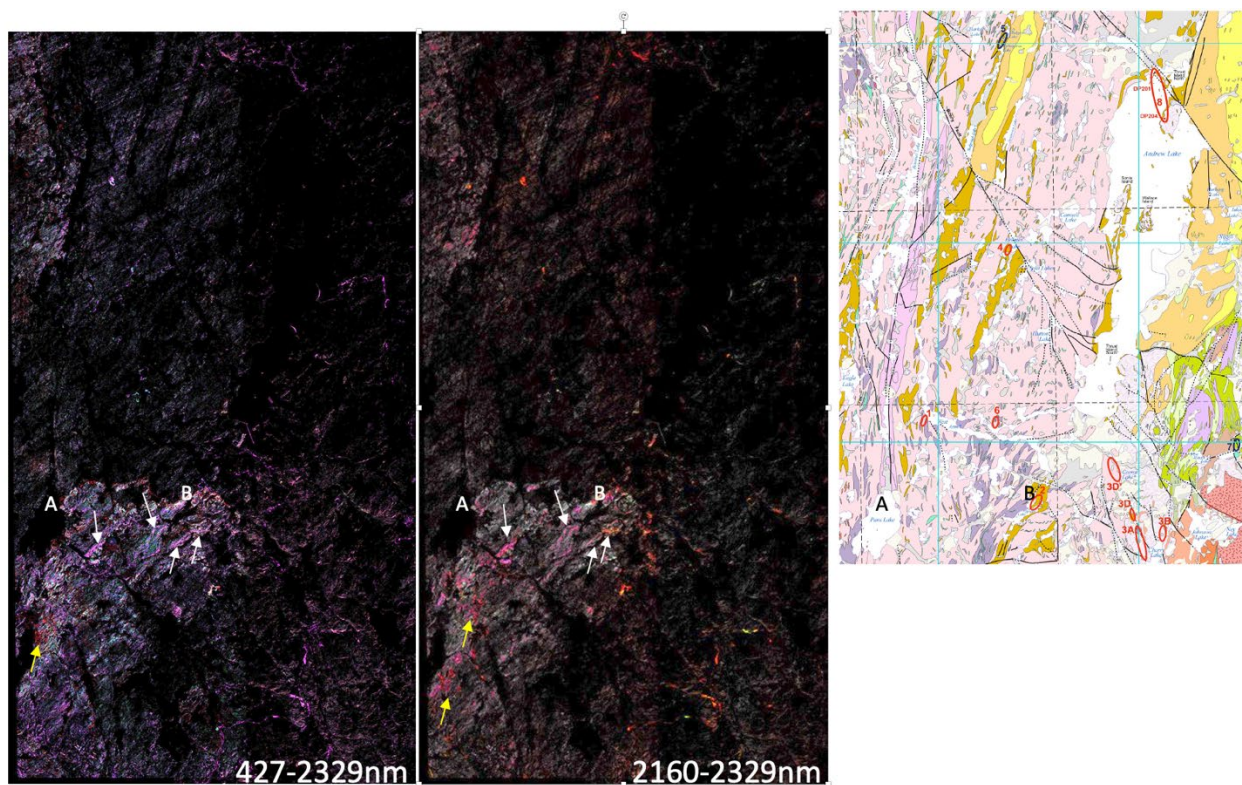


Figure 13. Comparison of spectral angle maps (SAM) derived from image endmembers and different spectral ranges, with the geological map approximately co-registered. White and black letters A and B act as reference point marking the location of Pans Lake and Spider Lake. The SAM map on the left was generated using the full spectral range (427-2329nm, all 16 bands) and a subset of the thirteen endmembers (EM 3,7,11 removed) to focus the analysis on differences in broad spectral shape amongst endmembers including the influence in the strength of iron features. The SAM map on the right was generated using the last four bands in the shortwave infrared and the 13 endmembers to focus the analysis on variations in the strength of hydroxyl features amongst endmembers. Image elements highlighted by yellow and white arrows are discussed in the text.

An enlargement of the shortwave infrared SAM map is shown in Figure 14 to gain an insight into the lithological significance of fine outcrop patterns (lenses) seen in Figure 13 with a focus on three areas capturing the three main colors in the image. Red pixels seen in area 1 lie outside of the map coverage. Magenta and orange pixels are predominant in areas 2 and 3 respectively and though it is difficult to establish a direct correlation with the geological map, the primary occurrence of magenta pixels is in the northwest of Spider Lake in contrast with orange pixel in the east of the lake suggesting they follow the map patterns of the hornblende granodiorite (purple map unit) and Rutledge River Complex (brown map unit) respectively. If so, this could be a useful finding as the Rutledge River Complex is known to host radioactive anomalies (e.g. red oval labeled 2 the on geologic map shown in Figure 14). Note that areas with red, magenta, and orange pixels encompass the following endmember sets in order of decreasing abundance indicating that they are indeed distinct and likely highlight differences in abundance of ferromagnesian and white mica minerals: red = EM 1,7,8; magenta= 6,1,7; orange= 1,4,8.

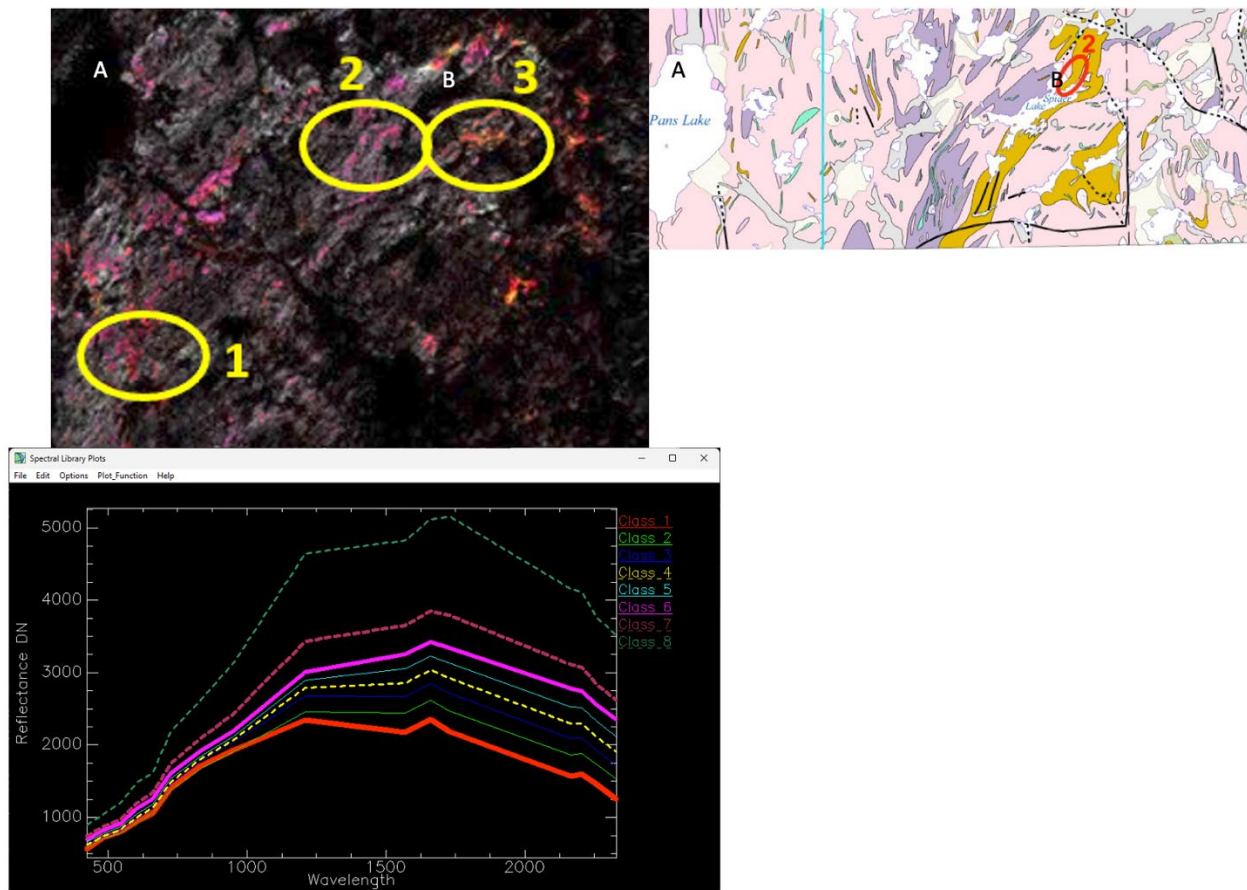


Figure 14. Enlargement from the SAM map (SWIR range) shown on Figure 13 along with partial coverage of the geological map and a plot of a subset of the thirteen image endmembers used to discuss outcrops seen in areas 1, 2, and 3 encompassing red, magenta, and orange pixels respectively. A and B mark the location of Pans Lake and Spider Lake.

4.5 Possible links between map units and Halo (field spectra) endmember maps

Field reflectance spectra can be extremely valuable for the detection of specific rock units if they are representative. They are a complement to image endmembers intended for data exploration to capture spectra of rocks that were not measured in the field either because of logistical constraints or simply because of a lack of knowledge of their existence. Here, due to time constraints, we make use of a limited subset of available spectra collected in the field in 2023. Eight Halo reflectance spectra shown on Figure 15 were selected to capture a range of spectral characteristics and reflectance amplitude. Several encompass hydroxyl features in the shortwave infrared attributable in part to white mica, biotite, and chlorite whose presence and absorption strength influence the shape of the resampled spectra in the last four bands (right frame in Figure 15).

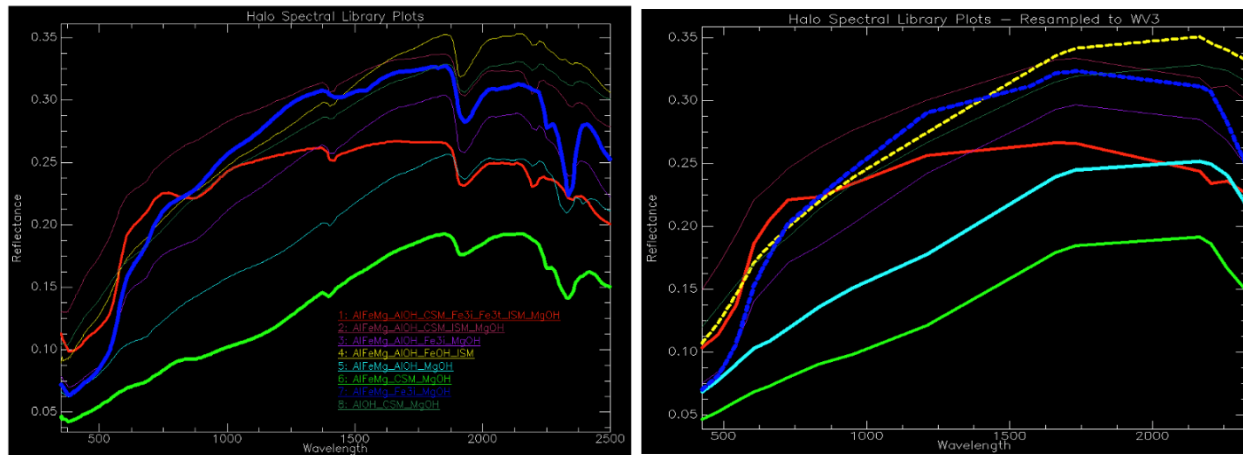


Figure 15. Eight Halo reflectance spectra (left) selected to capture a range of spectral characteristics and reflectance amplitude and equivalent spectra after resampling to WorldView-3 bandpasses (right). Note several hydroxyl features in the shortwave infrared attributable in part to white mica, biotite, and chlorite whose presence and absorption strength influence the shape of the resampled spectra in the last four bands.

The SAM map on the left on Figure 16 bears a strong resemblance to the index maps, particularly that of the WM/Chl-Bio and Rock MF suggesting that the eight spectra selected capture the overall spectral variability in the scene and can also be used for quick exploration of the data across the region. The SAM map on the right (SWIR bands) is more informative and begins to isolate outcrop patterns seen in Figure 14 (Areas 2 and 3) and may indicate that a more detailed exploration of the field spectra could help to further map the distributions of varying schist, and hornblende bearing felsic rocks in that part of the map.

Lastly four yellow arrows are shown on the top of the SAM map on the right (SWIR bands). The left most yellow arrow captures the extension of the Rutledge River Complex outcrops highlighted in the western part of Figure 10. The two arrows further south also capture outcrops within large map units of the same complex. The upper most arrow (furthest east) delineates two clear continuous strips of outcrops that have no corresponding mapped outcrops of the Rutledge River Complex. These findings suggest that some of the Halo spectra could be effective at highlighting rocks of this formation.

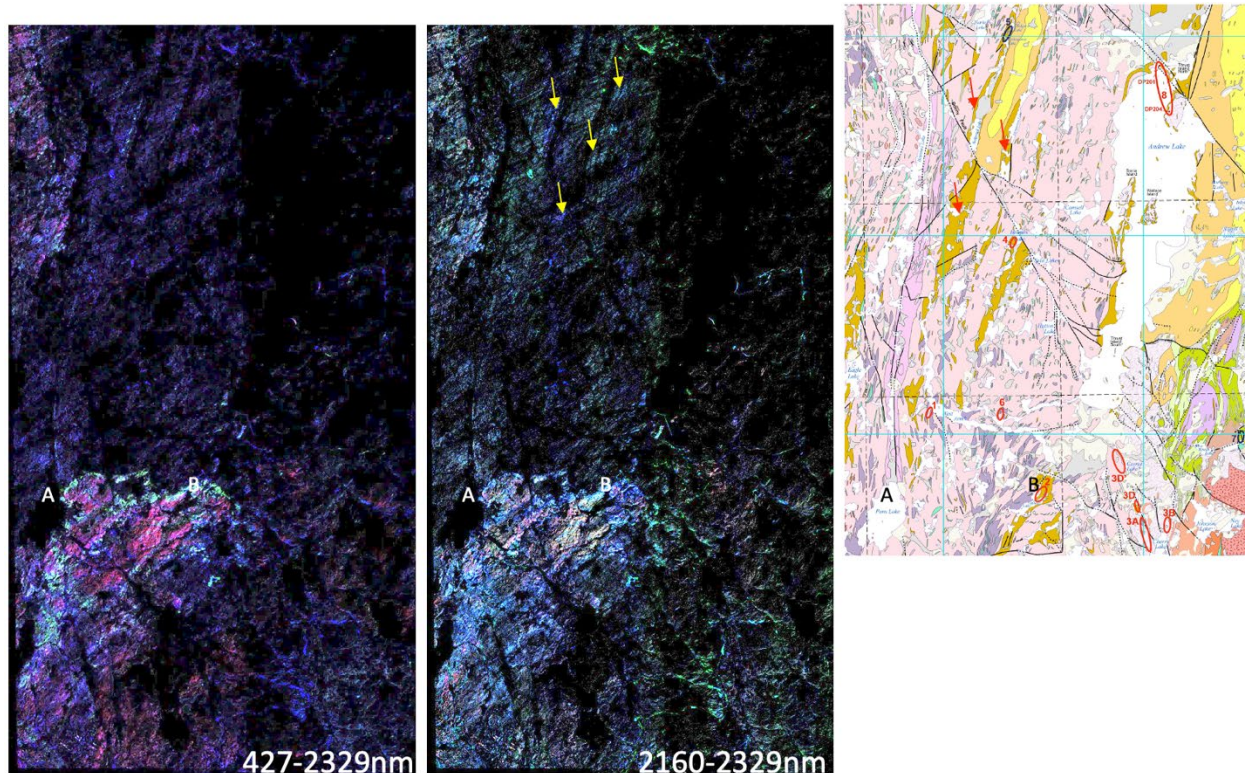


Figure 16. Comparison of spectral angle maps (SAM) derived from the eight Halo spectra (see Figure 15) and different spectral ranges, with the geological map approximately co-registered. The SAM map on the left (427-2329nm, all 16 bands) and on the right (2160-2329nm, 4 bands) made use of all eight spectra shown on Figure 15.

5. DISCUSSION AND CONCLUSION

5.1 Image acquisition

As per the prior 2023 study for Leland Lake (AER/AGS Special Report 116), considerable effort was spent preprocessing the two WorldView-3 images to isolate the portions of the scene occupied by outcrop and minimize, as best as possible, the influence of vegetation and shadows. In this respect the October 2021 scene, covering the eastern portion of the imaged area, enabled the capture of outcrops to a much lower extent than the June 2022 scene and likely indicates that lower solar illumination and the presence of leaf litter on outcrop hampered the acquisition of quality data. It is noteworthy that a September 22, 2022, scene in the Leland Lakes area yielded good results (AER/AGS Special Report 116). Thus, there is uncertainty as to how late in the fall one can expect to get good data for outcrop extraction, but October may be too late.

5.2 Lithological inferences

For this study, the lack of detailed geological mapping largely impeded firm lithological interpretations from the satellite data, specifically because most interpretations pointed to map units (amphibolites, Rutledge River Complex, hornblende rich gneisses) that are conveyed with varying detail on the available map. For example, regarding the Rutledge River Complex, Panã and Prior (2010, page 5) state that the “Complex consists of mappable bands and unmappable lenses of migmatite scattered throughout the granite gneiss. The migmatite complex consists of gneiss and schists... and small amphibolite and mafic lenses”. The index images (WM/Chl-Bio, White Mica, Rock MF), the SAM maps derived from image endmembers

and a subset of field spectra reveal diverse image domain particularly in the southwest and northwest portions of the area where the geologic map portrays larger domains of three map units: Hornblende granodiorite, amphibolite, and Rutledge River Complex. Because the range of image processing methods emphasize the detection of mafic minerals and white mica, most lithological inferences made here are tied to these three map units. Given the challenges of working without detailed maps, field validation is highly recommended should the methods be used to generate imagery to trace the distribution of any map unit or guide exploration strategies.

6. REFERENCES

- Godfrey, J.D. 1958. Mineralization in the Andrew, Waugh and Johnson lakes area, northeastern Alberta; Research Council of Alberta, Alberta Geological Survey, Earth Sciences Report 1958-04, 17 p.
- Godfrey, J.D. 1961. Geology of the Andrew Lake, north district, Alberta; Research Council of Alberta, Alberta Geological Survey, Earth Sciences Report 1958-03, 32 p.
- Godfrey, J.D. 1963. Geology of the Andrew Lake, south district, Alberta; Research Council of Alberta, Alberta Geological Survey, Earth Sciences Report 1961-02, 30 p.
- Langenberg, C.W. and Eccles, D.R. 1996. Metallic mineral occurrences of the exposed Precambrian shield in northeastern Alberta; Alberta Energy and Utilities Board, EUB/AGS Bulletin 64, 71 p.
- Mars, J.C. 2018. Mineral and lithologic mapping capability of WorldView 3 data at Mountain Pass, California, using true- and false-color composite images, band ratios, and logical operator algorithms. *Economic Geology*, v. 113, no. 7, 1587–1601
- Panã, D.I., and Prior, G.J. 2010. Geology of uranium and other mineral occurrences in the Andrew Lake area, Canadian Shield, northeastern Alberta (NTS 74M/16). ERCB/AGS Open File Report 2010-08, 39 p.
- Price, J. C. 1994. How unique are spectral signatures? *Remote Sensing of Environment*, 49, 181–186.
- Rivard, B. 2023. Analysis of WorldView-3 satellite imagery for the Leland Lakes area, Alberta. AER/AGS Special Report 116, 20 pages.
- Rogge, D., Bachmann, M., Rivard, B., and Feng, J. 2012. Spatial sub-sampling using local endmembers for adapting OSP and SSEE for large-scale hyperspectral surveys. *IEEE Journal of Selected Topics in Applied Earth Observations and Remote Sensing*, 5, 183–195.
- Rogge, D., Rivard, B., Zhang, J., Harris, J., Feng, J., and Sanchez, A. 2007. Integration of spatial-spectral information for the improved extraction of endmembers. *Rem. Sens. Environ.* 110(3), 287-303.
- Shedlovska, Y.I., and Hnatushenko, V.V. 2019. Shadow Removal Algorithm for Remote Sensing Imagery. *IEEE 39th International Conference on Electronics and Nanotechnology (ELNANO)*, pp. 818-822. DOI:[10.1109/ELNANO.2019.8783642](https://doi.org/10.1109/ELNANO.2019.8783642)

7. APPENDIX 1: List of digital deliverables

Georeferenced mosaic data for the following products are provided in ENVI format and in Geotiff format for visually enhanced products. JPG formatted files are also available for quick view.

Product	File name
1.Outcrop map	AndrewLake_Outcrop (envi)
2.SAM map of Image endmembers (2165-2500 nm)	SAM-EM13-2165-2500 (envi, img, rule)
3.SAM map of Image endmembers (350-2500 nm)	SAM-EM13-Full (envi, img, rule)
4.Rock FE index image	AndrewLake_Rock Fe (envi, geotiff)
5.Rock WM/Chl-Bio index image	AndrewLake_WM/Chl-Bio (envi, geotiff)
6.White Mica index image	AndrewLake_OH (envi, geotiff)
7.Rock MF index image	AndrewLake_Rock_MF 1 (envi, geotiff)
8.SAM map of Halo endmembers (2165-2500 nm)	Halo-SAM-2160-2330 (envi, img, rule)
9.SAM map of Halo endmembers (350-2500 nm)	Halo-SAM-Full1 (envi, img, rule)
10.Image endmember spectra library	Lib-ImageEM-13Selected (envi, lib)
11.Halo endmember spectra library	Halo-selected (envi, lib)